Rapid thermal chemical vapor deposition of zirconium oxide for metal-oxide-semiconductor field effect transistor application

Jane P. Chang, You-Sheng Lin and Karen Chu

Citation: Journal of Vacuum Science & Technology B: Microelectronics and Nanometer Structures Processing, Measurement, and Phenomena **19**, 1782 (2001); doi: 10.1116/1.1396639

View online: https://doi.org/10.1116/1.1396639

View Table of Contents: https://avs.scitation.org/toc/jvn/19/5

Published by the American Institute of Physics

Rapid thermal chemical vapor deposition of zirconium oxide for metal-oxide-semiconductor field effect transistor application

Jane P. Chang, You-Sheng Lin, and Karen Chu
Department of Chemical Engineering, University of California, Los Angeles, California 90095

(Received 7 December 2000; accepted 2 July 2001)

ZrO_2 is investigated in this work to replace SiO_2 as the gate dielectric material in metal-oxide-semiconductor devices for its high dielectric constant, good thermal stability on silicon, and large band gap. ZrO_2 films were deposited on p-Si(100) wafers by a rapid thermal chemical vapor deposition process using a zirconium (IV) t-butoxide $Zr(OC_4H_9)_4$ precursor and oxygen. At temperatures between 300 and 400 °C, the reaction was thermally activated with an activation energy of 29 kcal/mol, consistent with a β-hydride elimination mechanism leading to ZrO_2 deposition. In this regime at substrate temperatures below 350 °C, one atomic layer of ZrO_2 can be deposited after each alternating exposure to the precursor and oxygen, ideal for achieving conformal coverage of ZrO_2 over high aspect ratio features. Stoichiometric, uniform, and amorphous ZrO_2 was obtained, and highly conformal step coverage of the deposited ZrO_2 was observed on 300 nm features with an aspect ratio of 4. The dielectric constant of ZrO_2 achieved in this work ranged from 15 to 18 depending upon process conditions and small $C-V$ hysteresis and low interfacial state density were observed, ideal for metal-oxide-semiconductor field effect transistor application. [DOI: 10.1116/1.1396639]

I. INTRODUCTION

The fundamental limit of using SiO_2 as an insulator for the transistor gate dielectric is best illustrated by the world's smallest and practical transistor developed by Bell Labs researchers[1,2] where a transistor is built on 10–12 Å thick SiO_2 formed by rapid thermal oxidation of epi-silicon. The physical thickness of these ultrathin SiO_2 films sets limits for silicon based dielectrics: below this thickness range, the direct quantum-mechanical tunneling results in unacceptably high leakage current, and the breakdown of the dielectric happens at unacceptably low voltages.[3] Clearly, thicker dielectric films with higher permittivity than SiO_2 or silicon nitride (or oxynitride)[4–9] are needed to reduce the leakage current while maintaining acceptable gate capacitance, to continue increasing the silicon-based transistor's switching speed, and to accommodate the increasing complexity of ultralarge scale integrated circuits. In addition, other material considerations, such as the thermal and interfacial reactions, and band gap and barrier height of the dielectrics are critical for the required structural stability and low gate leakage currents. The transition to a nonsilicon-based dielectric also represents a fundamental change in processing towards deposited dielectrics and away from dielectrics that can be thermally grown on bulk or polycrystalline silicon. Deposited dielectrics must have excellent step coverage, thickness uniformity, and a precise control of interface properties which can only be attained through a thorough understanding of the surface reaction kinetics.

Potential high-k dielectric materials with a dielectric constant ranging from 10 to 100 include transition metal oxides (Ta_2O_5,TiO_2),[10–12] Al_2O_3,[13] ZrO_2,[14] HfO_2,[15] ferroelectric materials (e.g., $Pb(Zr,Ti)O_3$, $(Ba,Sr)TiO_3$),[16–19] and silicates ($ZrSi_xO_y$,$HfSi_xO_y$).[19] These materials also have applications as capacitors in rf circuits and/or in dynamic random access memory (DRAM) devices.[20] Rapid thermal processing has been widely used in semiconductor manufacturing for thermal oxidation/nitridation, deposition, annealing, ultrashallow junction formation, silicide formation, and borophosphosilicate glass reflow. Rapid thermal chemical vapor deposition (RT-CVD)[21,22] has emerged as a ''must'' technology to explore the high-k dielectric deposition for gate dielectric application where the quality and properties of the dielectric materials are most critical. The advantage of RT-CVD over other deposition techniques such as physical sputtering of various metal targets with oxygen containing gases, (plasma enhanced-) chemical vapor deposition with organometallic precursors, and molecular beam epitaxy, is the reduced thermal budget and improved control of the interfacial properties. These are achieved by rapidly ramping and precisely controlling the substrate temperature at which precursor gas molecules interact with the surface, undergo chemical reactions, and form the desired metal oxides/nitrides/carbides. Rapid thermal annealing[23,24] has been shown to be effective in annihilating the interfacial and bulk defects in these high-k materials.

We studied ZrO_2 deposition and its application in microelectronic devices since ZrO_2 is predicted to be thermodynamically stable[25] on silicon and has a high dielectric constant (15–22), high breakdown field (15–20 MV/cm), and large band gap (5–7 eV). Moreover, zirconium dioxide is the only thermodynamically stable solid form of zirconium with a simple fluorite structure. It may exist in either monoclinic (<1170 °C), tetragonal (1170–2370 °C), or cubic (2370–2680 °C) crystalline structures. At high temperatures, phase transformation from cubic or monoclinic to tetragonal structure has been reported,[26,27] with corresponding marked change in the electrical conductivity.[28,29] For metal-oxide-semiconductor field effect transistor (MOSFET) application,

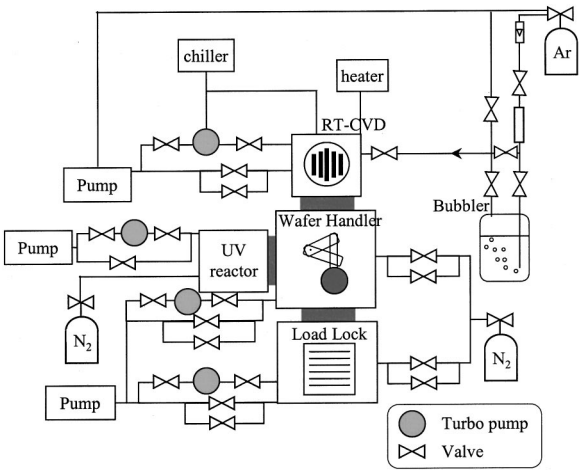

FIG. 1. Schematic diagram of the integrated system consisting a load lock, a transfer chamber, a UV photoreactor, and a RT-CVD system. The bubbler setup for the delivery of ZTB precursors is also shown.

an amorphous ZrO_2 film is preferred to prevent the leakage current through the crystallite grain boundaries. As to its electrical property, zirconium oxide is oxygen deficient when nonstoichiometric, therefore the predominant defects have been proposed to be oxygen ion vacancies.[30,31] In this work, MOS capacitors are built to assess the applicability of ZrO_2 as the gate dielectric materials in MOSFET devices.

II. EXPERIMENTAL SETUP

The RT-CVD of ZrO_2 was carried out in an integrated clustered system shown in Fig. 1. The system consisted of a load lock chamber for sample loading, unloading and storage, a central quartz robotic arm for transferring wafers in between chambers, an ultraviolet photoreactor for cleaning silicon surfaces prior to gate dielectric growth or deposition, and a rapid thermal reactor for thermal oxidation, chemical vapor deposition, or annealing. The concept of interfacing these reaction/process chambers allows integrated chemical processing of a single wafer to minimize the ambient contamination, extend process flexibility in integration, and reduce the processing error costs. Wafers ranging from 4 to 8 in. can be processed in this system.

The RT-CVD system is evacuated by a 1000 l/s turbomolecular pump to a base pressure of 2×10^{-8} Torr. A linear array of seven tungsten-halogen lamps is situated above the top quartz window to provide radiation and heating to the wafer. A N_2-cooled gold reflector is used to maximize the radiation into the reactor through the quartz window. The wafer is positioned on three quartz pins and is rotated at about 20 rpm to enhance the heating uniformity. An Ircon optical pyrometer is used to monitor the sample temperature during the deposition and its temperature readings are calibrated with bare silicon wafers embedded with a type K thermal couple.

We used zirconium t-butoxide (ZTB), $Zr(OC_4H_9)_4$, as the depositing organometallic precursor. This liquid precursor obtained from Strem Chemicals is slightly yellow with 99.99% purity. ZTB was chosen for its higher vapor pressure than other zirconium alkoixdes or $ZrCl_4$,[32] and it has been used to deposit ZrO_2 films.[32–34] In this work, ZTB was used in a bubbler setup where high purity argon (99.999%) was used to carry the ZTB vapor into the RT-CVD chamber. The bubbler was normally kept at room temperature but the gas line and reactor wall were heated to 50 °C. The deposition was carried out with ZTB and O_2 sequentially: ZTB was fed into the chamber at a pressure of 2×10^{-4} Torr for a set period of time, and the chamber was evacuated to its base pressure, followed by oxygen exposure for a certain period of time. The exposure time of ZTB and O_2 can be adjusted independently and the cycling of these two chemistries can be repeated until the desired thin film thickness is obtained. Note that the substrate temperature during ZTB and O_2 exposure can also be varied independently. In this study, ZrO_2 were deposited on 4, 6 or 8 in. *p*-type silicon (100) samples with 1–10 Ω cm resistivity, pre-cleaned with HF and then dried with dry N_2.

The compositional analysis was performed by x-ray photoelectron spectroscopy (XPS) using a monochromatic Al $K\alpha$ x-ray at 1486.6 eV, with a pass energy at 23.5 eV and a takeoff angle of 45°. The deposited film thickness was determined by a spectroscopic ellipsometer, along with the refractive index and extinction coefficient by modeling the spectra using single or multilayer thin film stacks.

The surface roughness was determined by a Nanoscope III Dimension 5000 (Digital Instruments) atomic force microscopy (AFM), with a silicon tip (<10 nm) in the tapping mode. The instrument was calibrated against National Institute of Standards and Technology traceable standards with an accuracy better than 2%. The crystallinity of the film was measured by x-ray diffractometer with Cu $K\alpha$ radiation at 64 keV. The infrared (IR) analysis was performed with both *s*- and *p*-polarized light source in a single transmission mode at 60° incident angle at room temperature with a DTGS infrared detector. Note that for the IR analysis, the substrates were 4 in. double-side polished float zone *n*-type silicon with a resistivity of 10 Ω cm.

To address the applicability of metal oxides as gate dielectric, MOS capacitors were fabricated by physical vapor deposition of 200 nm of aluminum on the deposited ZrO_2 film, followed by photolithographic patterning of the aluminum into top electrodes with electrode areas of 2×10^{-4} cm^2. The $C-V$ responses were measured by a HP 4145B probe station at 1 MHz.

III. RESULTS AND DISCUSSION

The Arrhenius plot of the reaction indicates the transition from a surface reaction limited deposition regime to a flux and decomposition limited regime as the substrate temperature increased (Fig. 2). At temperatures below 300 °C, no ZrO_2 deposition nor SiO_2 growth was observed during the deposition, as determined by both XPS and ellipsometry. At temperatures between 300 and 400 °C, the reaction was thermally activated with an activation energy of 29 kcal/mol. This activation energy is consistent with a β-hydride elimi-

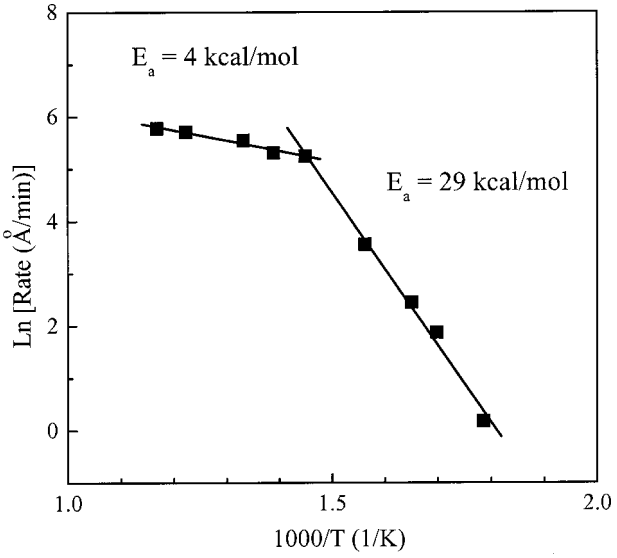

FIG. 2. Arrhenius plot of rapid thermal chemical vapor deposition of ZrO_2, illustrating the reaction limited regime with an activation energy of 29 kcal/mol, and a flux and decomposition limited regime with an activation energy of 4 kcal/mol.

nation mechanism reported for the decomposition of ethoxy groups following the adsorption of tetraethoxysilane[35] and the decomposition of t-butoxy species following the adsorption of ZTB on hydroxylated surfaces.[36] In this regime at substrate temperatures below 350 °C, one atomic layer of ZrO_2 can be deposited after each alternating exposure of the precursor and oxygen, as shown in Fig. 3. The linear scaling of deposition thickness as number of cycles indicated a good atomic layer controlled deposition, ideal for achieving conformal coverage of ZrO_2 over high aspect ratio features. At temperatures above 400 °C, the increase in deposition rate was reduced with an apparent activation energy of 4 kcal/mol due to decomposition and desorption of the precursors.

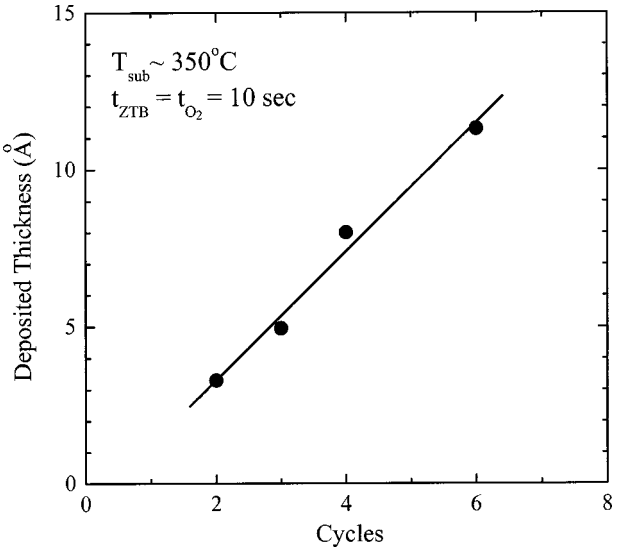

FIG. 3. Highly scalable atomic layer deposition of ZrO_2 as the number of ZTB and O_2 exposure cycles increased.

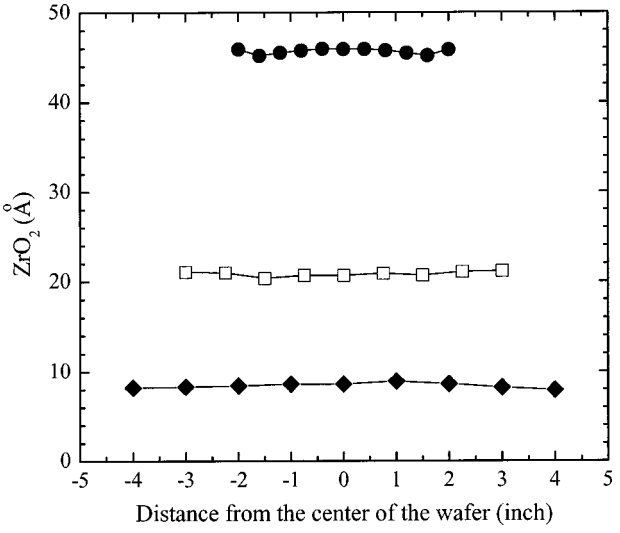

FIG. 4. Uniformity of deposited ZrO_2 on 4–8 in. silicon wafers, as measured by ellipsometry.

We also found that the deposited thin film thickness depended linearly on the precursor exposure time, the vapor pressure of the precursor (by heating of the bubbler), and the temperature of the substrate, but was not affected by the prolonged oxygen exposure time. The oxygen exposure at elevated temperatures (~550 °C) densified the film and removed carbon in the film, as determined by XPS analysis.

Highly uniform, ultrathin (5–100 Å) ZrO_2 was deposited on 4, 6 and 8 in. wafers by controlling the substrate temperature, as shown in Fig. 4. The thickness variation across a 4 or 8 in. wafer was less than 0.5%, as measured by ellipsometry with at least 20 measurement points taken from the wafer. The index of refraction was determined to be 2.1 ± 0.2, fairly close to the literature reported value of 2.16 and 2.19 for tetragonal and cubic ZrO_2,[37] and also similar to the value of 2.24 reported for monoclinic ZrO_2.[38] Therefore the crystalline structure cannot be derived directly from the refractive index measurement. The crystalline structure of the deposited ZrO_2 was further analyzed by x-ray diffraction (XRD) with Cu $K\alpha 1$ radiation and the collected spectra were compared to the available data from International Center for Diffraction Data.[39] The diffraction spectra, though not illustrated, showed only strong silicon diffraction lines with no other features, indicating the ZrO_2 film was either amorphous or had nano-crystallites on the order of or less than ten unit cells. Though monoclinic (110) and (011) and cubic (111) lines have been suggested in CVD deposited ZrO_2 films,[36] our XRD analysis suggested that amorphous ZrO_2 films were deposited. The deposited films were highly smooth as determined by AFM. The root-mean-square roughness was approximately 1–2 Å, as shown in Fig. 5.

The XPS compositional analysis shown in Fig. 6 used $Si^0(2p)$ at 99.4 eV as the reference binding energy for all spectra collected. Since the film thicknesses were less than 50 Å, XPS was capable of probing the entire film and its interface with the silicon substrate nondestructively. The $Zr(3d)$ spectra showed fully oxidized zirconium in its +4

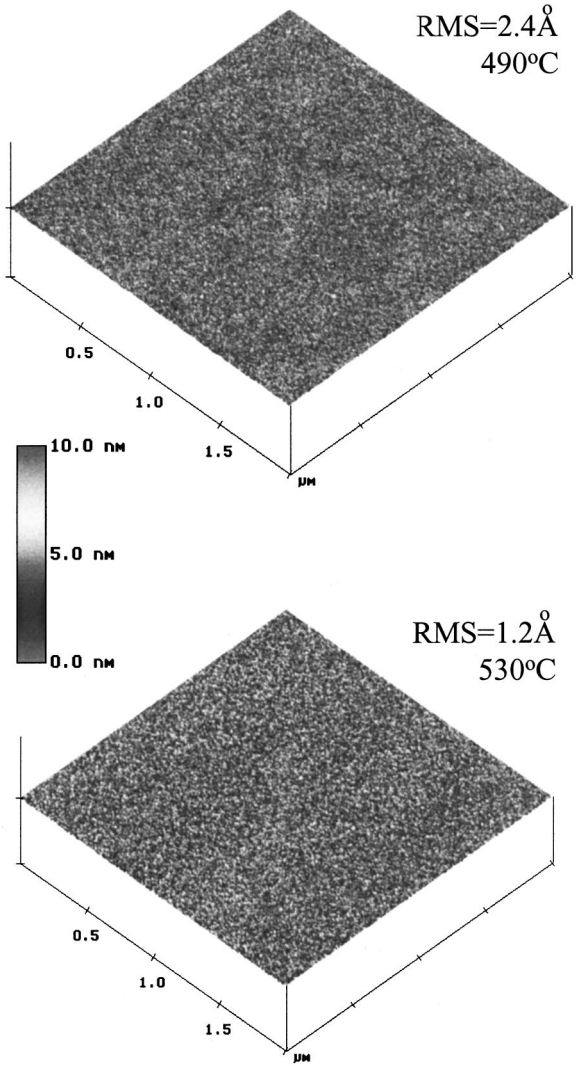

FIG. 5. Surface roughness of ZrO_2 films deposited at different temperatures, as measured by atomic force microscopy.

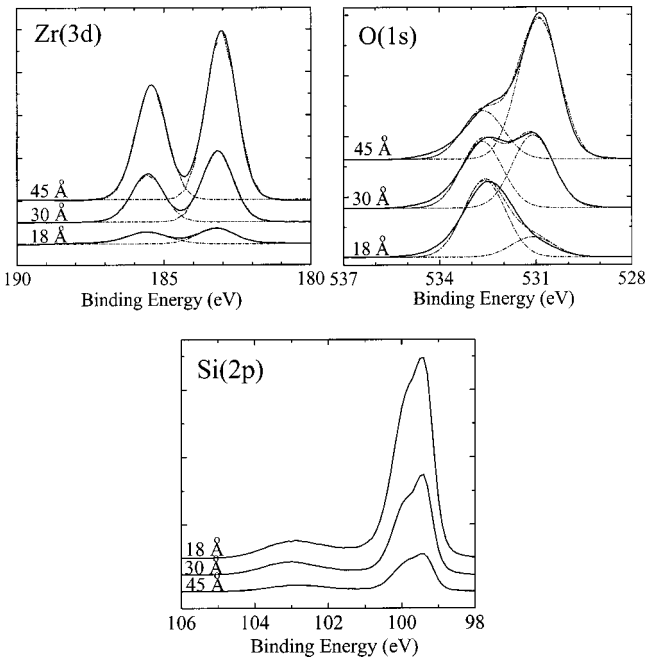

FIG. 6. X-ray photoemission spectra of Zr($3d$), O($1s$), and Si($2p$) from as-deposited ZrO_2 thin films on silicon. The thicknesses were measured by ellipsometry.

state, and the peak intensity increase as a function of the increasing ZrO_2 film thickness was consistent with a uniform overlayer model.[40] No substoichiometric zirconium oxide was observed. The O($1s$) spectra showed Zr–O bonding at 531 eV and C–O bonding at 532.5 eV. The Zr–O peak intensity also increased with the increasing film thickness, while the C–O peak intensity remained fairly constant. To confirm that the C–O peak in the O($1s$) spectra and the C($1s$) spectra obtained are due to surface contamination from ambient exposure, the surface was lightly sputtered by 1 keV Ar^+ ions and analyzed *in situ* by XPS. The adventitious surface carbon was quickly removed by Ar^+ sputtering and the bulk carbon concentration was determined to be negligible. Note that Si–O bonding should have a peak at a binding energy close to 532.5 eV in the O($1s$) spectrum, however, it was not deconvoluted explicitly due to its very low intensity (confirmed in the Si($2p$) spectra). The Si($2p$) spectra showed a strong $Si^0(2p)$ peak at 99.4 eV corresponding to the silicon substrate. From the attenuation of the $Si^0(2p)$ signal and a mean free path of photoelectron in ZrO_2 as 3 nm, we can calculate the ZrO_2 thickness which agreed well with the ellipsometric measurements. An additional peak at 102.8 eV corresponded to the formation of either substoichiometric silicon oxides or metal silicate. We have attempted to etch the ZrO_2 film and the interfacial layer with concentrated HF (49%), and found the interfacial layer highly resistant to the HF etching. This suggested that the interfacial layer was metal silicate with high chemical resistance but not SiO_x which should have dissolved easily in HF. More discussion of this interfacial layer, including high resolution transmission electron microscopy and compositional profiling, is detailed elsewhere.[41] The atomic concentration was determined by normalizing the integrated photoemission intensity of each element to its atomic sensitivity factor. The atomic ratio of Zr:O was determined to be nearly stoichiometric.

The deposited ZrO_2 was thermally stable on Si after annealing the film at 750 °C in ultrahigh vacuum followed by an *in situ* XPS analysis, as shown in Fig. 7. The Zr($3d$) spectra indicated that the ZrO_2 film remained fully oxidized and stoichiometric, and we observed a slight upward binding energy shift (~0.2 eV) which could be attributed to minor changes in local chemical coordination, possibly in the second-nearest neighbors. This 0.2 eV upward energy shift was also observed in the oxidized Si($2p$) peaks. No significant changes were observed in the O($1s$) or C($1s$) spectra after the annealing, thus the results are not shown. XRD analysis was performed on these high temperature annealed samples and yielded unchanged diffraction spectra, indicating that the films remained amorphous.

As hydrogen content cannot be quantified by XPS, IR analysis was carried out to determine the hydrogen incorpo-

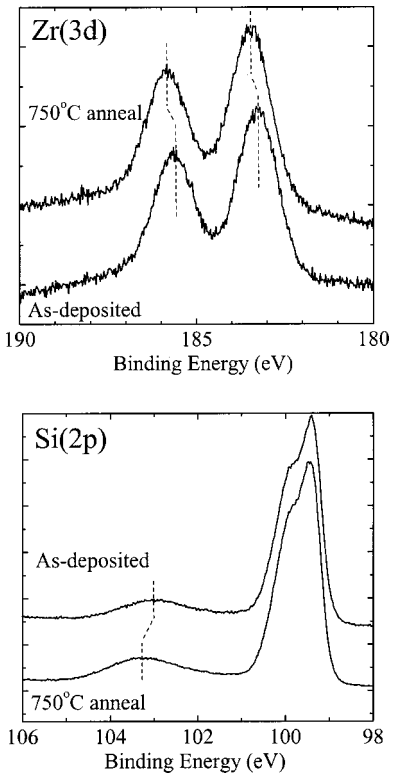

FIG. 7. Evolution of XPS Zr($3d$) and Si($2p$) spectra before and after *in situ* ultrahigh vacuum annealing of the ZrO_2 sample to 750 °C.

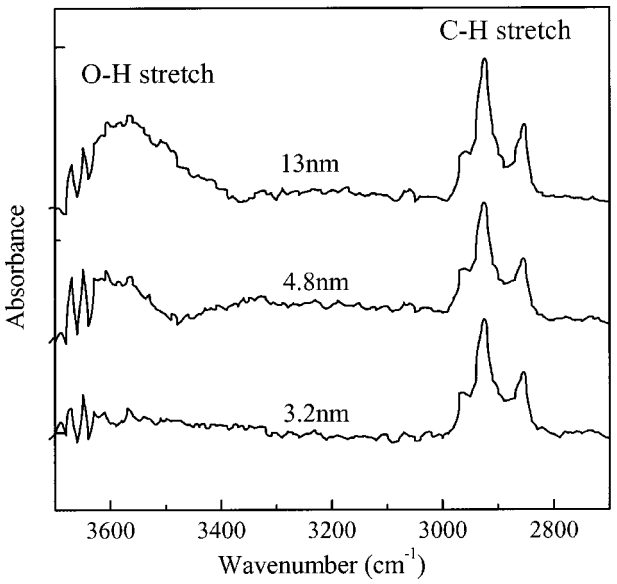

FIG. 8. Infrared spectra of O–H and C–H stretching vibrations in ZrO_2 films at various thicknesses.

ration in the film. The *ex situ* single transmission infrared analysis revealed O–H stretching vibration at 3200–3700 cm^{-1} and the C–H stretching vibration peaked at 2920 cm^{-1}. The integrated absorbance of O–H stretching vibration scaled proportionally with the film thickness while the integrated absorbance of C–H stretching vibration remained constant regardless of the film thickness, as shown in Fig. 8. All these samples were deposited at 410–420 °C. The result suggested that most of the hydrocarbon contamination was on the surface due to air exposure and packaging, while the OH groups were in the film and their intensities increased with increasing film thicknesses. The observed O–H vibrational mode was essential in the β-hydride elimination process[35] and its importance was confirmed by measuring twice as much ZTB adsorbed on a hydroxylated ZrO_2 surface compared to a dehydroxylated ZrO_2 surface.[36] In the β-hydride elimination process, ZTB precursor first adsorbed on the surface via a hydroxyl group and eliminated t-butanol, and the remaining t-butoxy species underwent β-hydride elimination to produce isobutylene and generate new hydroxyl groups on the ZrO_2 surface. Additional ZTB can thus be adsorbed on these newly generated hydroxyl groups. This explains why well-controlled atomic deposition was achieved in this work as the surface reaction was limited by the regeneration of reactive sites on the surface in the low temperature regime. The presence of OH and its intensity increase as the film thickness increased could be explained by the steric hindrance of ZTB molecules on available surface hydroxyl groups, leaving some OH groups un-reacted in the film.

Based on the measured deposition rates and the precursor pressure during the deposition, the ZTB reactive sticking coefficient was calculated to be $\sim 10^{-4}$, consistent with the literature reported value.[36] Highly conformal deposition was expected with these calculated low reactive sticking coefficients, therefore ZrO_2 was deposited on amorphous silicon trenches at 300 nm spacings with aspect ratios of 4. The cross sectional scanning electron micrograph in Fig. 9 illustrated the trench profiles before and after the ZrO_2 deposition. Excellent conformal step coverage was observed on these nanometer scale features with high aspect ratios, ideal for device application where dielectrics are needed to cover complex topographic features with high aspect ratios. Detailed analyses of the evolution of the deposited profiles are compared with Monte Carlo simulation in a forthcoming article.[42]

The MOS capacitors built with deposited ZrO_2 showed very low leakage current compared to thermally grown SiO_2 films, yielding 10^{-3} A/cm^2 at -1.5 V with an equivalent oxide thickness of 20 Å. From the capacitance–voltage measurements, good inversion was observed with small $C-V$ hysteresis. The expected flatband voltage for a MOS capacitor with an aluminum top electrode and a 1–10 Ω cm p-type substrate ($N_A \sim 3\times 10^{15}\,cm^{-3}$) was -0.74 eV. The measured flatband voltage at -0.35 eV indicated negative fixed charge ($\sim 4\times 10^{12}\,cm^{-2}$) in the film. Using the high frequency $C-V$ measurement and Terman's method,[43] the dielectric constant and the interface state density were determined to be ~ 18 and $\sim 2\times 10^{11}\,cm^{-2}\,eV^{-1}$, respectively, suitable for high-k application in MOS devices.

IV. CONCLUSIONS

Stoichiometric, uniform, amorphous, and thermally stable ZrO_2 with a dielectric constant of 18 was deposited on

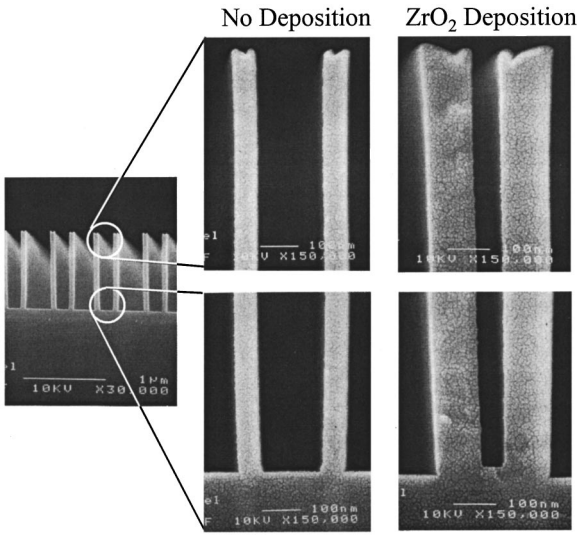

FIG. 9. Step coverage of ZrO_2 deposited over 300 nm trenches of amorphous silicon with aspect ratios of 4.

Si(100) wafers by a RT-CVD process using ZTB and oxygen. The two chemistries were introduced sequentially into the reactor with purging and evacuation in between. The deposition was surface reaction limited at temperatures between 300–450 °C. Excellent step coverage over 300 nm trenches with aspect ratios of 4 was observed. The MOS capacitors showed low leakage current, excellent $C-V$ responses, and low interfacial state density, ideal for MOSFET application.

ACKNOWLEDGMENTS

The authors would like to acknowledge Mattson Technology, Inc. (Steag CVD) for providing the patterned wafers for step coverage analysis and its financial support to this project. The financial contribution from the University of California Semiconductor Manufacturing Alliance of Research and Training (SMART) under the Award No. SM98-14 is also appreciated. The support from National Science Foundation (CTS-9985511) and UCLA Chancellor's Faculty Career Development Award are greatly appreciated. The authors are grateful for the technical assistance from Michael Sandler, Avishai Kepten, Robin Bloom, Sagy Levy, and Rodney Coffey at Steag CVD, and the IR analysis by Xiang Zhang and Yves Chabal at Bell Labs, Lucent Technologies.

Presented at the 47th International AVS Symposium, Boston, MA, 2–6 October 2000.

[1]D. Muller, T. Sorsch, S. Moccio, F. H. Baumann, E. Evans-Lutterodt, and G. Timp, Nature (London) **399**, 758 (1999).
[2]G. Timp *et al.*, Tech. Dig. Int. Electron Devices Meet. IEEE, Cat. No. 98CH36217, 1041 (1998).
[3]D. A. Buchanan, J. H. Stathis, E. Cartier, and D. J. DiMaria, Microelectron. Eng. **36**, 329 (1997).
[4]G. Lucovsky, J. Vac. Sci. Technol. A **16**, 356 (1998).
[5]E. P. Gusev, H. C. Lu, T. Gustafsson, E. Garfunkel, M. L. Green, and D. Brasen, J. Appl. Phys. **82**, 896 (1997).
[6]E. C. Carr, K. A. Ellis, and R. A. Buhrman, Appl. Phys. Lett. **66**, 1492 (1995).
[7]M. Bhat, L. K. Han, D. Wristers, J. Yan, and D. L. Kwong, Appl. Phys. Lett. **66**, 1225 (1995).
[8]Z. H. Lu, R. J. Hussey, M. J. Graham, R. Cao, and S. P. Tay, J. Vac. Sci. Technol. B **14**, 2882 (1996).
[9]T. P. Ma, IEEE Trans. Electron Devices **45**, 680 (1998).
[10]C. Chaneliere, J. L. Autran, R. A. B. Devine, and B. Balland, Mater. Sci. Eng., R. **22**, 269 (1998).
[11]G. B. Alers, R. M. Fleming, Y. H. Wong, B. Dennis, A. Pinczuk, G. Redinho, R. Urdahl, E. Ong, and S. Hasan, Appl. Phys. Lett. **72**, 1308 (1998).
[12]B. He, T. Ma, S. A. Campbell, and W. L. Gladfelter, Tech. Dig. Int. Electron Devices Meet. Cat. No. 98CH36217, 1038 (1998).
[13]L. Manchanda, W. H. Lee, J. E. Bower, F. H. Baumann, and W. L. Brown *et al.*, Tech. Dig. Int. Electron Devices Meet. IEEE, Cat. No. 98CH36217, 605 (1998).
[14]T. S. Jeon, J. M. White, and D. L. Kwong, Appl. Phys. Lett. **78**, 368 (2001).
[15]M Balog, M. Schieber, M. Michman, and S. Patai, J. Electrochem. Soc. **126**, 1203 (1979).
[16]B. van Dover, L. F. Schneemeyer, and R. M. Fleming, Nature (London) **392**, 162 (1998).
[17]R. A. Mckee, F. J. Walker, and M. F. Chisholm, Phys. Rev. Lett. **81**, 3014 (1998).
[18]J.-P. Han and T. P. Ma, Appl. Phys. Lett. **72**, 1185 (1998).
[19]G. D. Wilk and R. M. Wallace, Appl. Phys. Lett. **74**, 2854 (1999).
[20]J. P. Chang and Y.-S. Lin, J. Appl. Phys. **90**, 2964 (2001).
[21]K. Kobayyashi, Y. Inaba, T. Ogata, T. Katayama, H. Watanabe, Y. Matsui, and M. Hirayama, J. Electrochem. Soc. **143**, 1459 (1996).
[22]V. Misra, X. Xu, B. E. Hornung, R. T. Kuehn, D. S. Miles, J. R. Hauser, and J. J. Wortman, J. Electron. Mater. **25**, 527 (1996).
[23]S. O. Chung, J. W. Kim, S. T. Kim, G. H. Kim, and W. J. Lee, Mater. Chem. Phys. **53**, 60 (1998).
[24]Y. B. Hahn, J. W. Kim, C. J. Youn, and I. S. Lee, J. Electron. Mater. **26**, 1394 (1997).
[25]K. J. Hubbard and D. G. Schlom, J. Mater. Res. **11**, 2757 (1996).
[26]D. K. Smith and C. F. Cline, J. Am. Ceram. Soc. **45**, 249 (1962).
[27]C. T. Lynch, F. W. Vahldiek, and L. B. Robinson, J. Am. Ceram. Soc. **44**, 147 (1961).
[28]R. Kofstad and D. J. Ruzicka, J. Electrochem. Soc. **110**, 181 (1963).
[29]L. A. McClaine and C. P. Coppel, J. Electrochem. Soc. **113**, 80 (1966).
[30]C. R. A. Catlow, *Nonstoichiometric Oxides*, edited by O. T. Soresen (Academic, New York, 1981), Chap. 2, pp. 61–98.
[31]R. Ruh and H. J. Garrett, J. Am. Ceram. Soc. **50**, 257 (1967).
[32]Y. Takahashi, T. Kawae, and M. Nasu, J. Cryst. Growth **74**, 409 (1986).
[33]M. Matsuoka, S. Isotani, S. Miyake, Y. Setsuhara, K. Ogatam, and N. Kuratani, J. Appl. Phys. **80**, 1177 (1996).
[34]R. M. Brusasco, Proc. SPIE **1047**, 23 (1989).
[35]J. E. Crowell, L. L. Tedder, H. C. Cho, F. M. Cascarano, and M. A. Logan, J. Vac. Sci. Technol. A **8**, 1864 (1990).
[36]M. A. Cameron and S. M. George, Thin Solid Films **348**, 90 (1999).
[37]R. H. French, S. J. Glass, F. S. Ohuchi, Y. N. Xu and W. Y. Ching, Phys. Rev. B **49**, 5133 (1994).
[38]N. M. Balzaretti and J. A. H. da Jornada, Phys. Rev. B **52**, 9266 (1995).
[39]International Center for Diffraction Data, JCPDS Powder Diffraction File.
[40]D. Briggs and M. P. Seah, *Practical Surface Analysis, Vol. 1: Auger and X-ray Photoelectron Spectroscopy* Wiley, New York, 1990.
[41]J. P. Chang, Y.-S. Lin, S. Berger, A. Kepten, R. Bloom, and S. Levy, J. Vac. Sci. and Technol. B (submitted).
[42]J. P. Chang, Y.-S. Lin, and L. Sha (submitted).
[43]L. M. Terman, Solid-State Electron. **5**, 285 (1962).